Nonlinear absorption in Au films: Role of thermal effects

Nir Rotenberg,* A. D. Bristow,† Markus Pfeiffer, Markus Betz, and H. M. van Driel
Department of Physics, University of Toronto, Toronto, Ontario, Canada M5S 1A7
(Received 15 January 2007; revised manuscript received 1 March 2007; published 23 April 2007)

The effective nonlinear optical absorption coefficient β_{eff} is measured for 20-nm-thick Au films at 630 nm as a function of pulse width. The z-scan measurements show that β_{eff} increases from 6.8×10^{-7} to 6.7×10^{-5} cm W^{-1} as the pulse width is varied from 0.1 to 5.8 ps. To help interpret this $\sim100\times$ increase, differential transmission and reflectivity measurements are performed using 775 nm pump and 630 nm probe pulses. All experiments are simulated with a two-temperature model for electrons and lattice. The pulse width dependence of β_{eff} is consistent with thermal smearing of d-band to conduction-band transitions, with β_{eff} arising from changes in the linear (Im $\chi^{(1)}$) absorption coefficient.

DOI: 10.1103/PhysRevB.75.155426 PACS number(s): 78.20.Ci, 78.30.Er, 78.47.+p, 42.65.−k

I. INTRODUCTION

Thin metal films or nanoparticles have seen increasing use in areas such as nanoplasmonics,[1,2] photonics,[3,4] and metamaterials.[5,6] In particular, the strong nonlinear optical properties of metal systems have attracted considerable attention. The intensity (I) dependent absorption coefficient of a metal is normally discussed using the form $\alpha=\alpha_0+\beta_{\text{eff}}I$, where α_0 is the low-intensity, linear absorption coefficient and β_{eff} is the effective nonlinear absorption coefficient. Values of β_{eff} as high as[7,8] 10^{-2} cm/W have been reported, more than 10^6 times larger than that associated with other systems such as semiconductors where the dominant nonlinear absorption process is related to two-photon absorption, a component of Im $\chi^{(3)}$. Because of the form used for nonlinear absorption in metals, the β_{eff} is sometimes discussed in terms of a $\chi^{(3)}$ process, suggesting an intrinsic property and a nonlinear absorption process which only depends on pulse intensity. However, an indication that nonlinear absorption can depend strongly on other pulse parameters is evidenced by the fact that for Au films the value for β_{eff} measured at 530 nm using 25 ps pulses[7] and z-scan techniques is more than 2 orders of magnitude larger than that obtained at 600 nm with 100 fs pulses.[4]

The β_{eff} for metals in the midvisible region is actually attributable to thermal smearing of the electron distribution and its influence on linear absorption (Im $\chi^{(1)}$) associated with d-band to conduction-band transitions.[9,10] Some of the noted discrepancy in β_{eff} for Au can therefore be understood in terms of wavelength difference, since 530 nm is closer than 600 nm to the peak of the d-band to conduction-band transition at 510 nm. However, given the thermal origin for β_{eff}, other pulse parameters also play a role and, as shown below β_{eff}, may range over more than 2 orders of magnitude.

Here, we report experimental results from the investigation of the pulse width and intensity dependence of β_{eff} for 20 nm Au films using open-aperture transmission z-scans with 0.1–5.8 ps full width at half maximum (FWHM) 630 nm pulses. We also conduct pump-probe measurements to separately time resolve the reflectivity and transmission of the same sample at 630 nm. Simulations of the time-dependent electron temperature and optical properties are carried out using the two-temperature model (TTM) and are utilized to calibrate induced changes to the optical properties of Au. This is used to develop a self-consistent picture of the time-dependent and single-pulse (z-scan) effective absorption. It is shown that all data are consistent with the thermal smearing of the electron distribution and, hence, a pulse width and intensity dependence of Im $\chi^{(1)}$ (and β_{eff}) rather than with an intensity independent Im $\chi^{(3)}$ parameter. An Im $\chi^{(3)}$ component cannot be resolved by our experiment, given its sensitivity limits, and is likely much smaller than the thermally induced changes to Im $\chi^{(1)}$.

II. EXPERIMENT

For the experiments, several nearly identical Au samples are prepared by evaporating 99.9% Au onto a 1-mm-thick microscope slide with an evaporation rate of $\sim$1 nm/s. The films are approximately 20 nm thick with a thickness variation of $<10\%$, as determined by linear transmission and reflection spectroscopy (not given here). The films are partially transparent at a wavelength of 630 nm, for which the skin depth of Au is $\sim$15 nm.[11] z-scan and pump-probe experiments are performed using 630 nm, ultrashort pulses, obtained from a noncollinear optical parametric amplifier pumped by a 1 kHz Ti:sapphire laser amplifier.[12] Variable pulse widths are obtained using a double-pass, single grating pulse stretcher or a prism compressor to produce pulses in the range $0.1\leqslant\tau_p\leqslant6$ ps (FWHM), as measured using standard autocorrelation techniques. All pulses were verified to have Gaussian spatial and temporal profiles. The particular stretcher configuration is chosen over a four-pass stretcher in order to maintain sufficient pulse energy (all values are within 20% of 100 nJ) for the z-scan measurements. However, the two-pass configuration limits the maximum attainable pulse width to about 6 ps.

III. RESULTS AND DISCUSSION

A. z-scan

Open-aperture z-scan[13] measurements are performed in transmission, with the thin Au films scanned $\sim$10 mm through a focused beam created by a pair of 100 mm focal length lenses. The Rayleigh length (z_0) is approximately 1.5 mm with a minimum beam diameter (FWHM) of 40 μm.

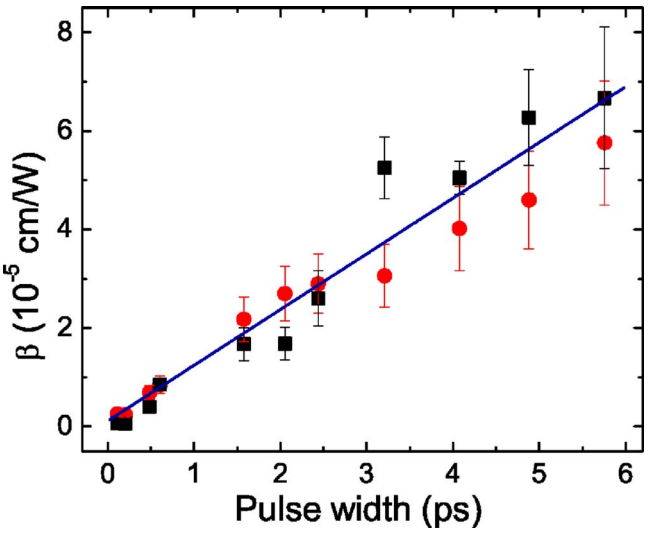

FIG. 1. (Color online) Pulse width (τ_p) dependence of nonlinear absorption coefficient β_{eff} (squares) extracted from the z-scan experiments and simulated values β_{sim} (circles) calculated from thermally induced changes to the linear absorption coefficient using the TTM. The line is a guide to the eyes.

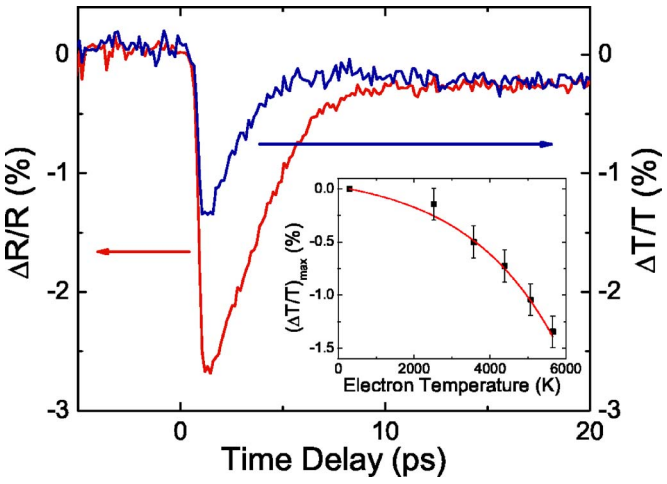

FIG. 2. (Color online) Time-dependent differential reflection (red) and transmission (blue) for a thin Au film pumped with a 200 fs, 775 nm pulse of fluence 5.3 mJ cm^{-2} and probed with 200 fs, 630 nm pulses. The inset shows the correlation between the $(\Delta T/T)_{\text{max}}$ measured experimentally (dots) for different excitation pulse fluences and the peak electron temperature at the Au front surface determined theoretically from the TTM.

A balanced detection scheme is employed to optimize the signal-to-noise ratio. The low pulse repetition rate ensures adequate time for heat dissipation between pulses to avoid thermal accumulation effects. The z-scan traces for the various pulse widths are fitted using the following expansion:[13]

$$T(z) = \sum_{m=0}^{\infty} \frac{\left[\dfrac{-\beta_{eff} I_0 L_{eff}}{1+\left(\dfrac{z}{z_0}\right)^2}\right]^m}{(m+1)^{3/2}}, \tag{1}$$

where L_{eff} is the effective optical path length in the sample. The extracted values are determined by fitting the individual z-scan traces with Eq. (1), with only four to five terms typically being necessary. Figure 1 shows the measured β_{eff} as a function of laser pulse width (FWHM). The data show that β_{eff} increases essentially linearly from 6.8×10^{-7} to 6.7×10^{-5} cm W^{-1} as the pulse width changes from 0.1 to 5.8 ps, a variation of nearly 2 orders of magnitude.

B. Pump-probe

In order to help understand how the absorption characteristics of our thin film are influenced by pulse width, it is necessary to understand how the optical properties vary with time following pulsed excitation. To obtain this, time-resolved pump-probe experiments are performed in both transmission and reflection geometries.[14,15] The Au film was excited by 200 fs, 775 nm pulses with fluence ranging from 1.0 to 5.3 mJ cm^{-2}. The induced changes in reflection and transmission are monitored using 200 fs pulses at 630 nm, the same wavelength as in the z-scan experiments; the probe pulse fluence is 65 μJ cm^{-2}. Differential transmissivity, $\frac{\Delta T}{T} = \frac{T-T_0}{T_0}$, and reflectivity, $\frac{\Delta R}{R} = \frac{R-R_0}{R_0}$, are obtained as a function of probe delay from measurements of the reflectivity or transmissivity for each delay time, with (R,T) and without (R_0,T_0) the pump pulse.

Figure 2 shows typical time-dependent $\Delta T/T$ and $\Delta R/R$ data for a Au film and excitation fluence of 5.3 mJ cm^{-2}; both $\Delta T/T$ and $\Delta R/R$ initially decrease as the pump pulse deposits energy into the electron system. The relative drop in the two signals is consistent with observations of Rosei *et al.* in thermomodulation experiments at the same wavelength.[9] Pumping leads to reduced Pauli blocking of conduction-band states and an increase in absorption. The electrons and probed optical properties partially recover on a time scale of ~5 ps, a time scale related to electron-lattice thermalization. As can be seen from Fig. 2, the recovery is not complete on a >10 ps time scale, since the lattice and electron temperatures are now at a (common) temperature of ~450 K following excitation.

While the overall optical response of the film can be understood in terms of temperature dynamics of the electrons, it is worth stating that the Fermi smearing mechanism, which is often used to model the temperature dependence of the reflection and transmission in metals near the peak of the d-band transition, is not complete at our probe wavelength, as acknowledged by Rosei *et al.* in their original paper.[9] In their model, the thermally induced change to the complex index of refraction for Au is based on a resonance in the absorption spectra caused by a single d-band transition at approximately 510 nm. For wavelengths >620 nm, their simple model actually predicts an increase in the transmission with a pump pulse incident, in contradiction to the experimental results presented here. Rosei *et al.* suggest that there are additional d-band transitions (associated with electrons in other regions of the Brillouin zone) that contribute to the change in the dielectric function; however, no quantitative assessment is given. These transitions are as yet unidentified, and, consequently, the thermally induced change of the

transmission and reflection cannot be accurately modeled far from 510 nm using this model, as is sometimes done in the literature. By providing actual pump-probe data to determine the electron temperature, a more direct means of evaluating the thermally induced changes in the optical properties is obtained.

C. Discussion

To relate the change in experimental transmission to electron temperature, we employ the TTM, which models the evolution of electron and lattice temperatures in metals due to ultrafast laser heating and has been successfully employed to understand optical properties of metals on a short time scale.[14–16] The TTM can be expressed through two coupled differential equations as follows:

$$C_e\frac{\partial T_e}{\partial t} = \frac{\partial}{\partial z}\left(K_e\frac{\partial T_e}{\partial z}\right) - g(T_e - T_\ell) + P(z,t),$$

$$C_\ell\frac{\partial T_\ell}{\partial t} = g(T_e - T_\ell),$$

$$P(z,t) = (1 - R_0)\alpha e^{-\alpha z} I(t), \tag{2}$$

where $C_{e(\ell)}$ is the electronic (lattice) heat capacity, $T_{e(\ell)}$ is the electron (lattice) temperature, K_e is the thermal conductivity of the electrons, g is the electron-phonon coupling constant of the metal, $P(z,t)$ is the generation term for energy density, R_0 is the experimentally determined linear reflectivity at room temperature, α is the linear absorption coefficient, and $I(t)=I_0\exp[-4(\ln 2)t^2/\tau_p^2]$ is the temporal intensity profile of a pulse of peak intensity I_0 and FWHM pulse width τ_p. Values of the parameters appropriate for our excitation conditions are obtained from Ref. 17. For pulses whose duration is as short as those considered here, thermal conduction effects can be neglected. We numerically solved these equations to obtain the time-dependent electron temperature at the surface of a Au film of our thickness when excited by a 200 fs pump pulse. We then correlated this time-dependent temperature to the experimental transmission change for a range of pulse fluence. The inset of Fig. 2 shows how the peak electron temperature is correlated to the maximum experimental differential transmission $(\Delta T/T)_{\max}$. It is interesting to relate the data in the inset to the transient transmission changes also displayed in Fig. 2. The transmission change of $\Delta T/T \sim -1.3\%$ observed for a delay time around 0.5 ps corresponds to a situation where the electrons have reached a peak temperature of 5600 K, whereas the lattice temperature is still close to the ambient value of 300 K. In contrast, for delay times >10 ps, the electrons and the lattice have equilibrated to a common temperature of ~ 450 K. The small (0.25%) residual transmission change might be partially related to lattice effects such as thermal expansion, which are not accounted for in the simulation.

From the above results, time-resolved carrier temperature profiles for pulses of various intensities or pulse widths can be computed from Eq. (2). This yields time-resolved differential transmission traces, as shown in Fig. 3. The transmitted probe fluence can then be evaluated numerically as

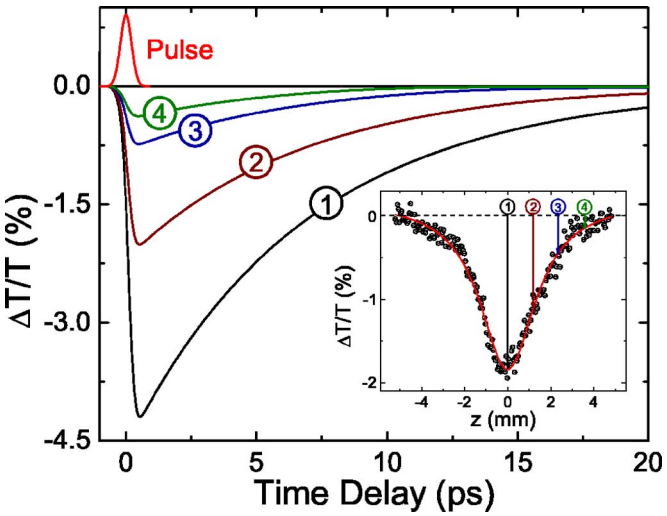

FIG. 3. (Color online) Simulated time-resolved transmissivity from two-temperature model calculations for a 630 nm, 600 fs pulse with 100 nJ energy and variable spot size. The focal spot diameter (FWHM) are $w_1=40$ μm, $w_2=60$ μm, $w_3=80$ μm, and $w_4=100$ μm. The inset shows an experimental z-scan trace (open circles) for the same pulse with corresponding fit (solid curve) using Eq. (1); the integers 1–4 in the inset correspond to the different beam diameters and indicate how a z-scan trace can be reconstructed from calculated thermally induced changes in optical properties.

$$F_T = \int_{-\infty}^{\infty} I(t)\frac{\Delta T}{T}(t)dt. \tag{3}$$

The total differential transmissivity due to thermal effects is then

$$\frac{\Delta T}{T} = \frac{F_T - F_0}{F_0}, \tag{4}$$

where $F_0=\sqrt{\pi}\tau_p I_0$ is the incident fluence.

An example of how these thermal effects can produce a z-scan trace is presented in Fig. 3. Here, $\Delta T/T(t)$ from a differential transmission measurement is shown for 600 fs pulses with different beam waists but constant peak power; the various focal spot diameters corresponding to different positions during an actual experimental z-scan measurement are shown in the inset. The integral given in Eq. (4) yields the highest transmitted fluence for the smallest beam waist (curve 1) and the lowest transmitted fluence for the largest beam waist (curve 4). Note that since this modeled z-scan profile follows the focusing of the beam and is therefore symmetric, each of curves 2–4 represent positions for both $\pm z$. Consequently, if one considers different beam waists and proceeds with the analysis presented above, one can reconstruct a z-scan trace based solely on the thermally induced change to the linear absorption; that is, the nonlinear behavior can be recovered from changes to Im $\chi^{(1)}$. At this stage of the simulation, we provide a prediction for the shape $\Delta T/T$ of a z-scan trace comparable to an experimental trace such as the one depicted in the inset of Fig. 3 for a 600 fs pulse.

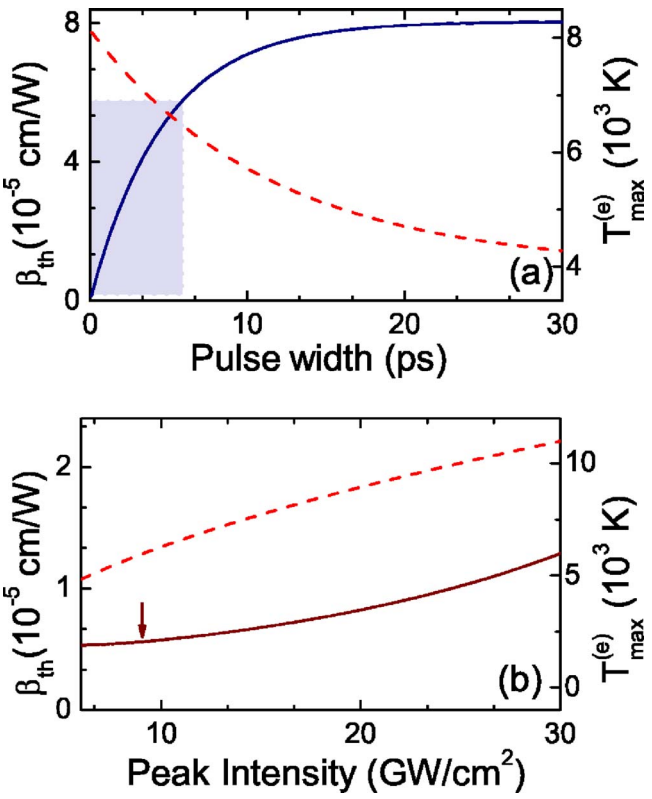

FIG. 4. (Color online) (a) Calculated β_{sim} as a function of pulse width for a pulse energy of 100 nJ, and a beam diameter of 40 μm. The shaded area indicates the range of conditions for which the experiments are performed. (b) β_{sim} as a function of peak pulse intensity for 500 fs pulses with a beam diameter of 40 μm. The intensity at which the z-scan was taken for this pulse length is shown with an arrow. The behavior of the peak electron temperature $T^{(e)}_{max}$, as a function of both parameters is plotted with the dashed line.

Then, we fit these data according to the standard z-scan formula [Eq. (1)]. This procedure gives a theoretical prediction for the nonlinear absorption coefficient β_{sim} as a function of the many pulse parameters. These values are presented in Fig. 1 and are in good agreement with the experimental data.

Figure 4(a) shows the simulated β_{sim} as well as the peak electron temperature at 630 nm as a function of pulse width for a pulse energy of 100 nJ and 40 μm spot size (FWHM), as used in the experiments. The curve has a dependence on pulse width that is approximately of the form $\beta_{max}(1-e^{-\tau_p/\tau_0})$, with τ_0=4.7 ps, but over the pulse width range considered in the experiments (shaded area), it is not strongly different from a linear behavior, in agreement with the data in Fig. 1. The constant τ_0 can be traced to the electron-lattice thermalization time, as indicated in Fig. 2. The maximum value of β_{sim} (obtained for $\tau_p \gg \tau_0$) is β_{max} $=8\times10^{-5}$ cm W^{-1}; note that higher pulse fluence would raise the maximum electron temperature, thus increasing both β_{max} and to a lesser extent τ_0, which depend on electron temperature, electron-lattice coupling constant, etc.[15] Figure 4(b) shows how β_{sim} varies with peak pulse intensity for a fixed pulse width of 500 fs. Over the range of intensities covered by the experiments (shaded area), one sees that β_{sim} increases slightly with intensity, reflecting the temperature dependence of material parameters such as electronic specific heat and electron-lattice coupling constant.[17] At low intensities, one expects and observes that β_{sim} becomes independent of pulse intensity at this pulse width. Overall, the theoretical behavior shown by the shaded region in Fig. 4(a), and those which cover conditions corresponding to the experiments, is in good agreement with the values of the experimentally determined β_{eff}, indicating that it is consistent with the thermal effects. Similar theoretical curves can be obtained for other probe wavelengths and indicate that the large value of β_{eff} obtained at[7] 530 nm is partly due to the large pulse width used, and, if Fig. 4(a) is a guide, the value obtained experimentally is near the maximum value possible.

Finally, it should be pointed out that we have defined and obtained the effective nonlinear absorption coefficient from z-scan measurements consistent with how this has been done in the literature for a metal. However, it should be noted that, to this point, the procedure presented only considers the changes in the transmissivity. Since the transmissivity, the reflectivity, and the absorption must sum to unity, the change in the total absorbance ΔA is

$$\Delta A = -(\Delta T + \Delta R). \tag{5}$$

Comparison of the induced reflectivity change with the induced transmissivity changes (Fig. 2) in the time-resolved experiments reveals that (i) both ΔT and ΔR are negative, leading to an increase of the absorption due to each effect, and (ii) the magnitude of ΔR is roughly twice that of ΔT. Consequently, the total change in the absorption for the Au film is about three times that previously obtained from the analysis of the transmissivity. In this sense, the effective nonlinear absorption coefficient of a metal has to be interpreted differently than that obtained from, for example, transmission z-scan data for a dielectric or semiconductor where changes to the reflectivity are negligible.

IV. CONCLUSION

In conclusion, the nonlinear absorption of Au films observed here, and likely that observed for other metal films, is dominated by thermally induced changes to the linear (Im $\chi^{(1)}$) absorption. The origin of this nonlinearity is believed to be a thermal smearing of electrons which inhibit the d-band to conduction-band transition and relax on a picosecond time scale. The pump-probe differential transmissivity and z-scan measurements, together with the two-temperature model, account for the nonlinear behavior. The effective nonlinear absorption coefficient β_{eff} widely used in the literature therefore has a pulse width dependence, since the induced absorption is based on a fluence and not on a strictly intensity dependent physical mechanism. While this is clearly shown here for Au at 630 nm, the results also likely apply to other metals at other wavelengths. Conversely, one can consider the effective nonlinear absorption coefficient to be a tunable parameter, so that by changing pulse parameters such as pulse width, intensity, or fluence, it is possible to change the coefficient by at least 2 orders of magnitude. If one varies the pulse wavelength, e.g., by tuning closer to the d-band to

conduction-band resonance, one can further increase the nonlinear coefficient by orders of magnitude.

ACKNOWLEDGMENTS

The authors thank Tak Sato for the preparation of the Au films and Tammy Lee for carrying out some of the preliminary measurements. Funding from the Natural Sciences and Engineering Research Council of Canada is greatly appreciated. N.R. acknowledges OGS for financial support and M.B. similarly acknowledges the Humboldt Foundation.

*Electronic address: nrotenbe@physics.utoronto.ca
†Present address: JILA, University of Colorado, 440 UCB, CO 80309-0440, USA.

[1] E. Ozbay, Science **311**, 189 (2006).
[2] W. L. Barnes, A. Dereux, and T. W. Ebbesen, Nature (London) **424**, 824 (2003).
[3] N. N. Lepeshkin, A. Schweinsberg, G. Piredda, R. S. Bennink, and R. W. Boyd, Phys. Rev. Lett. **93**, 123902 (2004).
[4] T. K. Lee, A. D. Bristow, J. Hubner, and H. M. van Driel, J. Opt. Soc. Am. B **23**, 2142 (2006).
[5] S. Linden, C. Enkrich, M. Wegener, J. Zhou, T. Koschny, and C. M. Soukoulis, Science **306**, 1351 (2004).
[6] J. B. Pendry, Science **306**, 1353 (2004).
[7] D. D. Smith, Y. Yoon, R. W. Boyd, J. K. Campbell, L. A. Baker, and R. M. Crooks, J. Appl. Phys. **86**, 6200 (1999).
[8] S. Debrus, J. Lafait, M. May, N. Pinçon, D. Prot, C. Sella, and J. Venturini, J. Appl. Phys. **88**, 4469 (2000).
[9] R. Rosei, F. Antonangeli, and U. M. Grassano, Surf. Sci. **37**, 689 (1973).
[10] F. Haché, D. Ricard, C. Flytzanis, and U. Kreibig, Appl. Phys. A: Solids Surf. **47**, 347 (1988).
[11] D. Aspnes, Thin Solid Films **89**, 249 (1982).
[12] E. Riedle, M. Beutter, S. Lochbrunner, J. Piel, S. Schenkel, S. Sporlein, and W. Zinth, Appl. Phys. B: Lasers Opt. **71**, 457 (2000).
[13] M. Sheik-Bahae, A. Said, T. Wei, D. Hagan, and E. W. van Stryland, IEEE J. Quantum Electron. **26**, 760 (1990).
[14] C.-K. Sun, F. Vallée, L. H. Acioli, E. P. Ippen, and J. G. Fujimoto, Phys. Rev. B **50**, 15337 (1994).
[15] H. E. Elsayed-Ali and T. Juhasz, Phys. Rev. B **47**, 13599 (1993).
[16] S. I. Anisimov, B. L. Kapeliovich, and T. L. Perel'man, Zh. Eksp. Teor. Fiz. **66**, 776 (1974) [Sov. Phys. JETP **39**, 375 (1974)].
[17] Z. Lin and L. V. Zhigilei, Proc. SPIE **6261**, 62610U (2006).